NIGERIAN ONLINE JOURNAL OF EDUCATIONAL SCIENCES AND TECHNOLOGY (NOJEST)

http://**nojest.unilag.edu.ng**

NIGERIAN ONLINE JOURNAL
OF
EDUCATIONAL SCIENCES
AND TECHNOLOGY

Extraction Of Feature For Efficient Analysis And Classification Of Biomedical Image

Ibrahim Musibau Adekunle
Department of Information and Communication Technology
Osun State University, Nigeria
Email: kunle ibrahim2001@yahoo.com

Oladotun Ojo
Department of Physics
Osun State University, Osogbo, Nigeria

To cite this article:

Musibau A. I. & Oladotun O. (2021). Extraction Of Feature For Efficient Analysis And Classification Of Biomedical Image. *Nigerian Online Journal of Educational Sciences and Technology (NOJEST), 3*(2), Pages 120-132

Nigerian Online Journal of Educational Sciences and Technology (NOJEST)

Volume 3, Number 2, 2021

Extraction Of Feature For Efficient Analysis And Classification Of Biomedical Image

Musibau A. I. & Oladotun O.

Article Info

Article History

Received:
29th January 2021

Accepted:
10 December 2021

Keywords
Biomedical, Higuchi dimension, Structural, Tissue image, multispectral spectrum

Abstract

The purpose of this paper is to demonstrate effectiveness and efficiency of different fusion techniques in the analysis and characterization of diseases pattern in medical images. Local features have been combined with global features of images to generate new descriptors or features for efficient characterization and classification of biomedical images. Some of the important research questions that would be specifically addressed in this paper include the following: What are the techniques for feature extractions? How can the fractal dimension be applied to detect different patterns in medical images? Can the combined features from both local and global features provide robust descriptors of shape/textures for the analysis and classification of image? Answers to these research questions would be illustrated with several experiments. Several methods of feature fusion techniques in the analysis of medical images have been suggested and evaluated in different ways. This paper proposes to develop new descriptors using fusion techniques to address some of the limitations of the existing methods in terms of efficiency, speed of image analysis and error corrections. Results analysis and some important implementation aspects of the new descriptors that could be used to improve the overall classification accuracy have been discussed in this paper. The performance measure of different models have been investigated using combined features for further improvement and analysis in detection and classification of Emphysema patterns.

Introduction

The research work reported in this paper uses several fundamental concepts in fractal theory. While fractals are commonly associated with self-similar objects, in image analysis applications, fractal measures represent certain types of irregularities in structures. The most fundamental measure that characterizes the scaling behaviour of a fractal structure is the fractal dimension. Several types of fractal dimensions and their computational aspects are discussed in this paper.

The notion of fractals is closely tied to several important geometrical concepts such as self-similarity, symmetry, periodicity and scale invariance. Some of the shapes that are commonly used as examples of fractals are the Koch curve, the Sierpinski triangle, the dragon curve and the Barnsley fern (Figure 1-1).The structural similarity at various levels of detail (or "scales") can be clearly observed in all the above shapes. Indeed, these shapes are generated using this very property. Given a shape at the base level, multiple copies are created, transformed and positioned according to a well-defined procedure to get the shape at the next level.The iterative process is repeated a number of times to get fractal shapes with the required level of complexity.

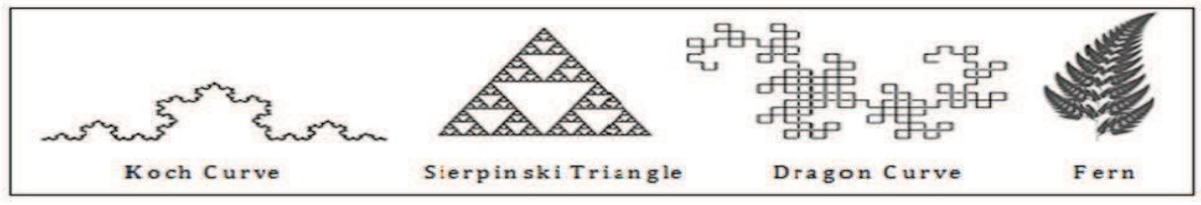

Two such iterative procedures are Linder Mayer system (L-system) and the iterated function system (IFS). The first three fractals in Figure 1-1 was generated using L-systems, while the Fern was generated using an IFS. The L-system uses a grammar based string production rule that generates a fractal as a string of turtle commands. The IFS on the other hand uses a set of affine transformations to repeatedly transform a point. The collection of all points thus generated forms a fractal shape.

There are more complex methods for generating fractals. The Mandelbrot set is defined as the orbit of a point at the origin under the iteration of a non-linear map of second degree in the space of complex numbers. When the generating point is switched to the constant value of the quadratic map, we get a group of interesting fractal shapes called Julia sets. Both the Mandelbrot and the Julia sets are highly intricate and infinitely complex shapes (Figure 1-2).

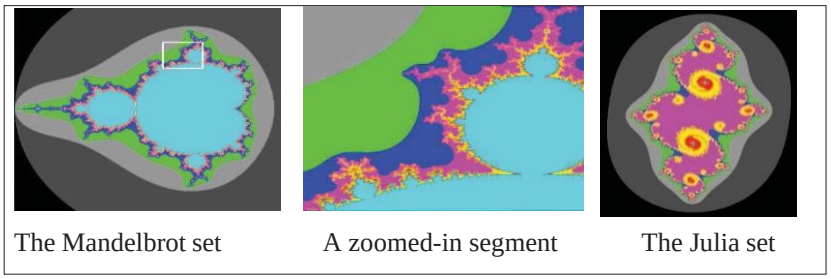

Figure 1-2: The Mandelbrot and the Julia sets

Inspired by the structural complexity and the aesthetic features of the Mandelbrot and Julia sets, several other popular fractal shapes were also developed using both complex and hyper-complex systems. These developments also saw the evolution of new areas such as fractal art side by side the development of fractal theory in mathematics and physics.

All fractals highlighted so far in this section fall into the general category of deterministic fractals. Another important class of fractals is based on stochastic rules or the inclusion of random variations in the iterative systems described above. A classic example of a one-dimensional random fractal is the Brownian motion obtained by integrating Gaussian white noise. Random fractals can be used to create models of several real-world objects and natural phenomena in computer by using graphics. Models of trees, terrains and clouds can be generated using random fractal processes, where the non-uniform appearance is created with the addition of random perturbations. A very well-known technique for generating random fractals is the mid-point displacement method. This method also finds applications in the diamond-square algorithm used for terrain programming.

Euclidean Dimension and Topological Dimension

One of the most commonly used dimensions is the Euclidean dimension D_E that considers the space occupied by an object. In this measurement, a structure is called one-dimensional if it is embedded on a straight line, two-dimensional if it is embedded on a plane and three-dimensional if it is embedded in space. A point has dimension 0. The topological dimension D_T of an object corresponds to the number of independent variables (or parameters) needed to describe it. Thus, a point is 0-dimensional, a curve is 1-dimensional, and spherical surfaces and planes have a topological dimension 2. The Euclidean and topological dimensions both assume only integer values.

Hausdoff Dimension

The notion of a fractal dimension is entirely based on the theory of Hausdoff dimension (also known as Hausdorff-Besicovitch dimension). Consider a curve C on a two-dimensional plane, which is covered using a set of discs D_j or radius r_j ($j = 1..n$) as shown in Figure 2-1. We impose the condition that $r_j \leq \delta$ for some $\delta > 0$, for all j. Such a set of discs is called a δ- cover of C.

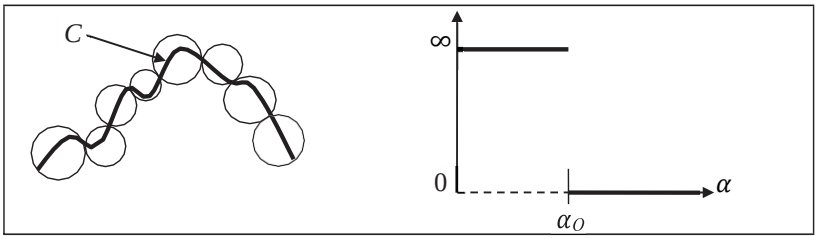

Figure 2: A δ -cover of a curve C, and a depiction of the Hausdorff dimension

The Hausdorff measure $H_\alpha(C)$ on the curve C is defined in terms of its δ- cover and a parameter (exponent) α as

$$Ha(C) = \frac{lim}{\delta \to 0}\{inf\left[\varepsilon_i r \frac{a}{j}\right]\} \qquad (2\text{-}1)$$

The Hausdorff measure has the property that there exists a critical value α_0 such that:

$$H_\alpha(C) = \infty, \text{ if } \alpha<\alpha_0$$
$$H_\alpha(C) = 0, \text{ if } \alpha>\alpha_0 \qquad (2\text{-}2)$$

The value of $\boldsymbol{\alpha_0}$ is called the Hausdorff dimension of the curve C.

Methods for Computing Fractal Dimension

Fractal dimension plays a central role in the theory of fractals and also in almost all applications involving fractals. Fractal dimension has the ability to characterize the irregularity of shapes, which other dimensions such as the topological dimension may not be able to represent. The fractal dimension is used to estimate the size and roughness of fractal sets; it is a number associated with a fractal that tells how densely the fractal occupies the underlying space.
The computational methods used for the estimation of fractal dimension in this paper are the box counting and the Higuchi methods. These and related methods are outlined in the following sections.

2.4 Box **counting Dimension**

Box counting is the most widely used fractal dimension in computing applications. It became a highly popular technique because it can be very easily implemented. Box dimension is also sometimes referred to as the capacity dimension. The definition is based on the concepts relating to δ-cover presented in this section. For computing the box dimension, we subdivide a rectangular region containing a fractal curve into sub-regions (or "boxes") of size δ.

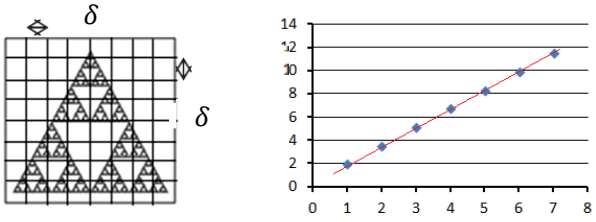

Figure 2-2: The regular subdivision and the linear regression used in box-counting algorithm.

If we denote the number of boxes of size δ that intersect a fractal curve C by $n_\delta(C)$, then the box-counting dimension of C is given by

$$D = \frac{lim}{\delta \to 0} \left[\frac{log_2 n_\delta(C)}{-log_2 \delta} \right]$$

The above method is usually implemented by iteratively halving the box size in each step, and counting the number of boxes that contain at least one point of the fractal. If N denotes the image size in each direction, the fractal dimension D is estimated as the slope of a linear regression line through the points on a log-log plot with $\log_2(N/\delta)$ along the x-axis and $\log_2(n\delta(C))$ along the y-axis (Figure 2-2). The values obtained for a Sierpinski triangle with image size $N = 256$ are shown in Table 2-1.

Table 2-1: Values generated by the box-counting algorithm for Sierpinski triangle.

δ	nδ (C)	$\log_2$(N/δ)	$\log_2$ nδ (C)
128	4	1	2
64	12	2	3.58496
32	36	3	5.16993
16	108	4	6.75489
8	324	5	8.33985
4	979	6	9.93517
2	2952	7	11.5275

2.4.1 Higuchi Dimension

The Higuchi's method is another efficient way of calculating the fractal dimension of a curve that has found several applications in the analysis of time series (Higuchi, 1988). Higuchi's method is particularly suitable for a one-dimensional signal whose values at regular discrete intervals are available in the form $x(i)$, i = 1, 2, ...N. Several new data point series are constructed using an interval length , and starting value index t:

$$S_t(\varphi) = \{x(t), x(t+\varphi), x(t+2\varphi), \ldots\ldots x(t+p\varphi)\} \qquad (2-4)$$

Where

$$p = [\tfrac{t-1}{\varphi}] \qquad (2\text{-}5)$$

The length of the series in (1-4) is calculated as a normalized sum of differences:

$$l_r(\varphi) = \frac{N-1}{P\varphi^2} \sum_{i1}^{p} I\, x(t+i\varphi) - x(t+(i-1)\varphi) \qquad (2\text{-}6)$$

The mean length for each interval length is obtained as

$$L(\varphi) = \frac{1}{\varphi} \sum_{\varphi}^{1} L_k(\varphi) \qquad (2-7)$$

As in the case of the box-counting dimension, the Higuchi dimension D_H is also computed as the slope of a linear regression line obtained using a log-log plot with log(φ) along the x-axis, and log (L(φ)) along the y-axis.

An *N*x*N* image *I*(*i*, *j*) must be converted to one-dimensional data before the above method can be applied. A common approach used for this is to add the values along each column to get a one-dimensional array of sums of pixel intensities:

$$x(i) = \sum_{j=1}^{N} I(i,j), j = 1,2, \dots N. \quad (2\text{-}8)$$

Generalized Renyi Dimension

The box-counting dimension outlined above can be extended to a generalized family of dimensions called Renyi dimensions. These dimensions use a probability measure functionμ. In the context of the box- counting algorithm, μ_i represents the probability of finding a point of the fractal within a box with index *i*. The Renyi dimensions D_q are defined with respect to a non-negative parameter q as

$$D_q = \frac{1}{q-1} \lim_{\delta \to 0} \frac{log_2[\sum_{i=1}^{N} \mu_i^q]}{log_2 \delta} \quad (2\text{-}9)$$

As a special case of the above, when q becomes 0, we get the box counting dimension. In a fractal system the measured object is assumed to have an internal structure with different spatial scales; the number N(e) of features of certain size e scale as (Posadas, 2003 & Martinez, 1999):

$$N(e) \sim e^{F} \quad (2\text{-}10)$$

Where F is the fractal dimension, which describes the scaling properties or the size distribution of 2D objects. The box counting method is used to obtain the scaling properties of the object by covering the measured object with boxes of size S and counting the number of boxes containing at least one pixel representing the object under study, N(S):

$$\mathrm{F}_0 = \lim_{s \to 0} \frac{\log N(s)}{\log(\frac{1}{s})} \quad (2\text{-}11)$$

The box counting dimension F_0 can be determined as the slope of the linear regression of log N(S) versus log (1/s) measured over a range of box sizes. The multi-fractal measure can be characterized through the scaling of the kth moments of Pi distribution in the form (Chhabra, 1989; Martinez, 1999 & Oiwa, 1998):

$$\Sigma_{\mathbf{i}=1}^{\mathrm{N}(\mathrm{S})} \mathrm{p}_{\mathbf{i}}^{\mathrm{k}}(\mathrm{S}) = \mathrm{S}^{(\mathrm{k}-1)\mathrm{Fk}} \quad (2\text{-}12)$$

where F_k is the generalized fractal dimension defined from Eq. (1-13) as:

$$\mathrm{F_k} = \lim_{s \to 0} \frac{1}{k-1} \frac{\log \sum_{i=1}^{N(s)} p_i^k(s)}{\log s} \quad (2.13)$$

The exponent in Eq. (2-12) is known as the mass exponent of the kth order moment ϯ(q) (Martinez, 1999 &Miranda, 2006):

(k) = (k-1)F_k (2-14)

As can be seen in Eq. (2-13), when k =0, all the boxes have a weight unity (Appleby, 1996 & Mendoza, 2010), the numerator becomes N(S) and the F_k becomes the capacity dimension, F_0 (Eq. (2-11). The other two special cases are when k = 1 and k =2 which are known as the information dimension F_1 and correlation dimension F_2 respectively. For k = 1, it can be derived from Eq. (2-13) as:

$$\mathrm{F}_1 = \lim_{s\to 0} \frac{\log \sum_{i=1}^{N(s)} pi \log pi}{\log s}$$

F_1 is directly related to the information or Shannon entropy (Thomazini, 2008 &Oudjemia, 2013), which quantifies the degree of disorder present in a distribution. For *k* = 2 the correlation dimension F_2 can be obtained as:

$$\mathrm{F}_2 = \lim_{s\to 0} \frac{\log \sum_{i=1}^{N(s)} pi^2}{\log s}$$

F2 is mathematically associated with the correlation function and computes the correlation of measures contained in intervals of size S. The fractal dimension of higher moments can be estimated according to Eq. (2-13). The Renyi spectrum is generated by the graphs of F_k versus k and it represents the mass distribution of an image. F_k addresses how mass varies with the e (resolution or box size) in an image. On the other hand, the plot of Fk for different values of k is called the generalized dimensional $F_2 \leq F_1 \leq F_0$, where the equality $F_0=F_1=F_2$ occurs only when the fractal is statistically or exactly self-similar and homogenous (stosic, 2006 & Zaia, 2006). According to [2-10], the singularity spectrum can be calculated using a set of real numbers k with the following equation:

$$\alpha(\mathrm{k}) = \lim_{s\to 0} \frac{\log \sum_{i=1}^{N(s)} \mu_i \log [pi(s)]}{\log s} \quad (2\text{-}17)$$

and the direct computation of $f(\alpha_k)$ value is :

$$\mathrm{f}(\alpha_\mathrm{k}) = \lim_{s\to 0} \frac{\log \sum_{i=1}^{N(s)} \mu_{i(k,s)} \log [\mu i(k,s)]}{\log s} \quad (2\text{-}18)$$

Where the quantities $\mu_i(k,s)$ are defined as

$$\mu_i(k,s) = \frac{p_i^k(s)}{\sum_{i=1}^{N(s)} p_i^k(s)} \quad (2\text{-}19)$$

$p_i(S)$ is the fraction or probability of the object contained in each ith box of size S.

Applications and Algorithms

In Section 1.2.3 above, we presented the Higuchi's method for computing the fractal dimension of an image. This method has become very popular due to its simplicity and speed of computation. The decomposition of a two-dimensional image into one-dimensional signals greatly helps in reducing the complexity of the algorithm. Two

fundamental fractal shapes were used, the Sierpinski triangle and the Sierpinski carpet (Figure 2-3) for our analysis of Higuchi's method.

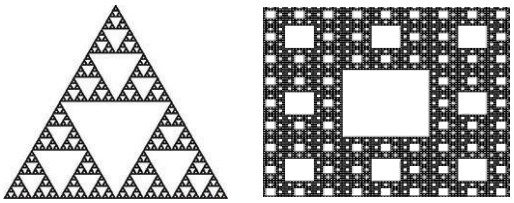

Figure 2-3: Images of the Sierpinski triangle and Sierpinski carpet used for the computation of Higuchi's dimension

The slopes of the linear regression of the log-log plots in Figure 2-4 gives the estimated fractal dimension of the Sierpinski carpet using the box counting method and the Higuchi's method.

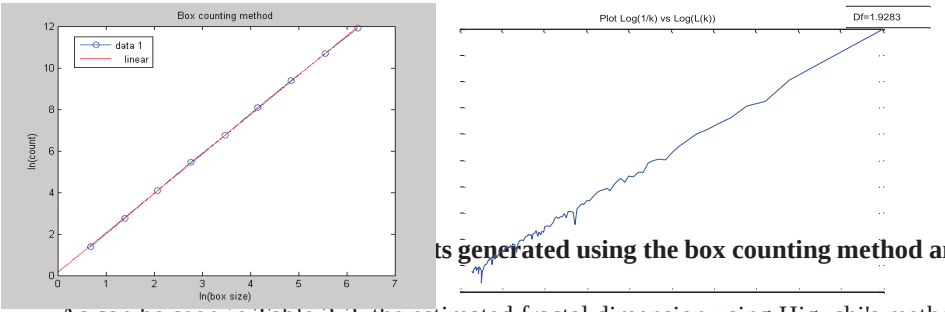

ts generated using the box counting method and Higuchi's method for the

As can be seen in Table 2-2, the estimated fractal dimension using Higuchi's method results deviates more from the theoretical FD with a p- value of 0.7995 compared to the box counting method with a p-value of 0.1857. This difference is attributed to the horizontal and vertical projections of image values used in the Higuchi's method. However, the two algorithms seem to perform well in general, and can be used for efficient computation of digital images since the estimated FD values are sufficiently close to the theoretical values.

	Box counting	Higuchi 's Method	Theoretical FD
Sierpinski Carpet	1.9013	1.9283	1.8928
Sierpinski Triangle	1.5673	1.6519	1.5850

Table 2-2: Estimation of fractal dimensions of fractal images

2.4 Parameter Selection for Higuchi's Algorithm

In Higuchi's algorithm, selection of k_{max} is very important in the estimation of fractal dimension as this parameter determines the performance of the algorithm. Few studies in the past have attempted to address the issue of k_{max} selection: the authors in (Accardo, Affinito, Carrozzi, & Bouquet, 1997) selected $k_{max} = 6$ as the optimum value. Other studies have suggested that the selection of the k_{max} range should probably be subjected to further consideration if a large N is to be used, that is, the authors suggested increasing k_{max} for increasing N. In another study (Paramanathan & Uthayakumar, 2008), the authors provided an algorithmic estimation of k_{max}, inspired by a divider method for FD estimation. In their approach, k_{max} of Higuchi's method was re-calculated for every FD estimation.

In our study, a wide range of k_{max} values was considered in the range 17-25. The image size $N=5l2$ was used. Using each of those values, the FDs using Higuchi's algorithm were calculated for different Weierstrass sequences. In order to generate Weierstrass sequences; a deterministic Weierstrass cosine function (Tricot, 1995), sampled at N equidistant points was used:

$W_H(x) = \lambda^{iH} \cos(2\Pi\lambda^i x) < H < 1$ (2-20)

Where t> *I* and, following (Esteller et al., 2001), and *x ‹ [0, l], N =5l2* was used. The above defined function is Weierstrass's example of a continuous function that is nowhere differentiable and has a known theoretical *FD*. More specifically, parameter *H* is connected to the theoretical *FD* (FD_{th}) of the Weierstrass function by $FD_{th} = 2\text{-}H$. Using (2-20), Weierstrass sequences, each having a different theoretical *FD* value (i.e. *l.l,l.2,l.3,...,l.9*), were generated. In order to evaluate the performance of the algorithm for different k_{max} values, a mean square error (*MSE*) was estimated according to (2-21).

$$MSE = \frac{1}{n}\sum_{i=1}^{n} FD_{th}(i) - FD_e(i))^2 \quad (2\text{-}21)$$

Where FD_{th} is the theoretical *FD* value for the images, FD_e is the estimated fractal dimension and n is the number of weierstrass sequences (of different theoretical *FD* values) used for the *MSE* estimation. Figure 2-5 shows the *MSE* against k_{max} (Higuchi steps); it reflects the performance of the algorithm with respect to *k*-values. As can be seen in the figure, when *k* ranges from 17 to 25, the *MSE* value is almost zero and this means the expected fractal dimension and the estimated fractal dimension at these points are almost the same. These values of k_{max} were considered in *FD* estimation using Higuchi's algorithm when applied to fractal images.

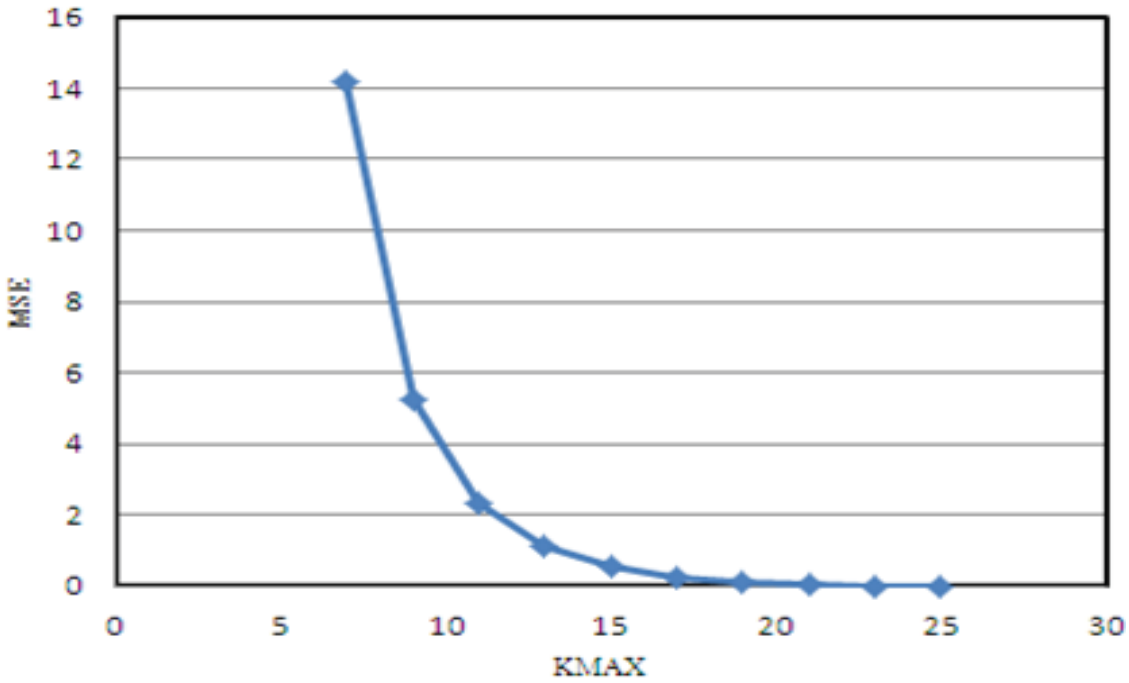

Figure 2-5: MSE for Higuchi's FD estimations for increasing KMAX values

The values of *k* less than *7* led to a poor performance, which resulted in very High *MSE* values. However, as the value of *k* increases from 7, the value of *MSE* decreases.

Holder Exponent Computation

Using the values of the intensity measures $\mu_P(r)$ described in the previous section, we can explore how they scale with *r* and establish the power laws satisfied by them.

$$\mu_P(r) = C\, r^{\alpha p}, \quad \alpha > 0. \quad (3\text{-}1)$$

where *C* is a constant of proportionality and α_P represents the Holder exponent for the power law of the measure under consideration at the point *P*.

As in the case of fractal dimension, the value of α_P is calculated as the slope of the linear regression line of the log-log plot where log(*r*) is plotted on the *x*-axis and log(μ) along *y*-axis. The linear regression lines and the corresponding values of α_P for the graphs are presented in Figure 3-1.

Figure 3-1: Graphs showing the computation of linear regression lines from log-log plots of measure values

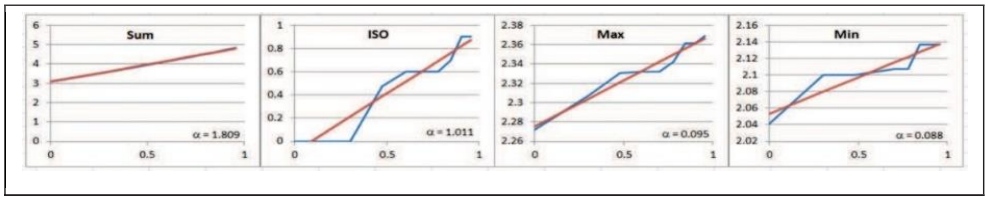

Since for every P, we get a value α_P of the Holder exponent for the chosen measure, we can form a rectangular array of values α_P having the same size as the original image. This two-dimensional array is called the α-image.

3.5 Multi-fractal Spectrum of Tissue Images

As mentioned in the previous section, the subdivision of the α range of an input image gives a decomposition of the image in terms of a set of α- slices. If we compute the fractal dimension of each of the α-slices, we get another powerful feature descriptor called the multi-fractal spectrum. The multi-fractal spectrum gives the variation of the fractal dimension with the Holder exponent α for a given intensity measure. It has been used as robust feature descriptors in image analysis applications including tissue image classification (Mukundan & Hemsley, 2010). An example of a tissue image and a multi-fractal spectrum computed from the image are shown in Figure 3-2.

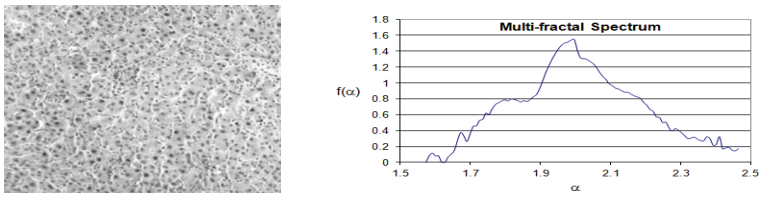

Figure 3-2: A tissue image and its multi-fractal spectrum

This spectrum was generated by subdividing the range of α values into 100 subintervals, with each of the 100 α-slices generating one fractal dimension. Fractal dimensions with magnitude less than 0.4 are generally considered insignificant and not used as part of any feature vector. Similarly, values of α_{min} and α_{max} are also chosen to eliminate the points at both ends of the fractal spectrum where high frequency oscillations are usually found.

The multi-fractal spectra computed for the tissue image in Figure 3-2 corresponding to the four intensity measures presented earlier in this section, are given below in Figure 3-3.

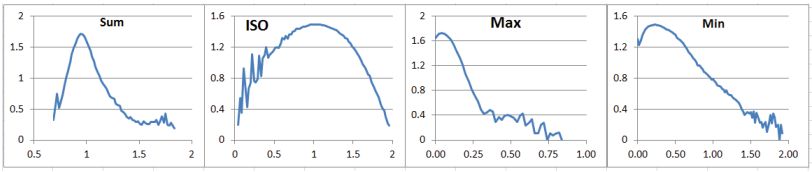

Figure 3-3: The multi-fractal spectra corresponding to four different intensity measures, computed for the input image in Figure 3-2.

Conclusions

Medical image analysis algorithms for automatic segmentation, extraction of regions of interest and classification based on features present in image have found useful applications as diagnostic tools in pathological assessments. This paper has presented several novel methods for emphysema classification and analysis of regions of interest using multi- fractal descriptors. The algorithms presented in this paper rely on several concepts from the theory of fractals. This paper has outlined some of the important properties of fractals such as self-similarity and

measures associated with them. The most widely used measure is the fractal dimension. This paper has discussed the essential concepts behind Hausdorff measures, box- counting dimension, Higuchi dimension and the generalized Renyi dimensions. The Renyi dimensions bear a close relationship with the multi- fractal spectrum of the measure μ. The next section gives an overview of concepts related to multi-fractal measures and the multi-fractal spectrum. Section 1 provided the theoretical foundations of fractals that are important in image processing applications, and discussed the mathematical aspects of different forms of fractal dimensions. Section 2 described some related features that could be used to reveal the intensity distributions of any natural image using fractal and multi-fractal properties. Some of the approaches outlined in this paper were implemented and applied for solving different problems in pattern analysis and classification. Section 3 introduced four key multi-fractal measures used in this paper, and described the computation of important multi-fractal features such as the alpha histogram, multi-fractal spectrum and Higuchi's dimension. Gaps in

existing research work such as the application of Higuchi dimension in medical image analysis have been identified and later used in this paper to develop new algorithms. Results showing inter-class variance and intra-class similarities in multi- fractal features demonstrated the effectiveness and discriminating power of the features in the analysis and classification of the lung CT images. This paper also presented different novel algorithms for the analysis of emphysema patterns using the Renyi spectrum features. In image classification problems involving large number of features, it is important to incorporate feature selection methods to improve the classification accuracy. Features such as the multi-fractal spectra, Renyi spectra and alpha-histograms can all contain large numbers of values. Overall, this research work has provided a significant number of contributions in the field of fractal and multi-fractal analysis of medical images, specifically for emphysema pattern classification.

References

Abraham, R., Simha, J. B., & Iyengar, S. S. (2008). Effective Discretization and Hybrid feature selection using Naïve Bayesian classifier for Medical datamining, *4*(2), 1–13.

Accardo, A., Affinito, M., Carrozzi, M., & Bouquet, F. (1997). Use of the fractal dimension for the analysis of electroencephalographic time series. *Biological Cybernetics*, *35O*, 339–350.

Agarwal, G., Mishra, S. P., Maurya, S., Chaudhary, S., & Murala, S. (2017). Local peak valley co-occurrence patterns: A new feature descriptor for image retrieval.*International Conference on Signal and Information Processing (IConSIP)*.

Agbazo, M.N., Goli G.K., Alamou E., Kounouheus B., & Afouda A. (2016). Scale invariance properties of rainfall in AMMA-CATCH observatory. Rev, Sci. Tcchnol, Synthese 33: 16-25.

Ahammer, H. (2011). Higuchi Dimension of Digital Images. *PLoS One*, *6*(9), 1–8. doi:10.1371/journal.pone.0024796

Ahonen, T. (2009). Rotation Invariant Image Description with Local. *Scia*, 61–70. doi:10.1007/978-3-642-02230-2_7

Appleby, S. (1996). Pattern of the Human Population. *Geographical Anaysis*, *28*(2), 147–160.

Atupelage, C., Nagahashi, H., Yamaguchi, M., Abe, T., & Hashiguchi, A. (2013). Computerized Medical Imaging and Graphics Computational grading of hepatocellular carcinoma using multi-fractal feature description. *Computerized Medical Imaging and Graphics*, *37*(1), 61–71. doi:10.1016/j.compmedimag.2012.10.001

Azim, T., & Niranjan, M. (2014). Texture Classification with Fisher Kernel Extracted from the Continuous Models of RBM. *Proc. Intnl. Conf. on Computer Vision Theory and Applications*.

Bahreini, L., Homayoun, J., & Gity, M. (2010). Classification of Breast Lesions in Dynamic Contrast - Enhanced MR Images. *Proceedings of the l7th Conference of Biomedical Engineering*, 1–4.

Bankier, A.A., Maertelaer, V.D., Keyzer, C., and Gevenois, P. A. (1999). Pulmonary emphysema: Subjective visual grading versus objective quantification with macroscopic morphometry and thin-section CT densitometry, *Radiology*, 211(3), 851–858.

Baravalle, G. B., Delrieux, C. A., & Gómez, J. C. (2015). Multifractal characterisation and classification of bread crumb digital images, *9*, 1– 10.

Berwald, J. J. (2011). Computing Multifractal Spectra Via Simplicial Measures.

Bhuvaneswari, R., & Kalaiselvi, K. (2012). Naive Bayesian Classification Approach in Healthcare Applications. *International Journal of Computer Science*, *3*(1), 106–112.

Block, A., von Bloh, W., & Schellnhuber, H. (1990). Efficient box- counting determination of generalized fractal dimensions. *Physical Review A*, *42*(4), 1869–1874. doi:10.1103/PhysRevA.42.1869

Block Imaging web portal. (2011). Retrieved June 6, 2017, from https://info.blockimaging.com/bid/70751/ge-lightspeed-qx-i-vs-ge- lightspeed-plus-ct-scanners

Blum, A. L., & Langley, P. (1997). Selection of relevant features and examples in machine learning. *Artificial Intelligence*. doi:10.1016/S0004-3702(97)00063-5

Breiman, L. (2001). Random forests. *Machine Learning*, *45*, 5–32. doi:10.1023/A:1010933404324

Broniatowski, M., & Mignot, P. (2001). A self-adaptive technique for the estimation of the multifractal spectrum. *Statistics & Probability Letters*, *54*(2), 125–135. doi:10.1016/S0167-7152(00)00210-8

Castiglioni, P., Rienzo, M. Di, Parati, G., & Faini, A. (2011). Fractal dimension of mean arterial pressure and heart-rate time series from ambulatory blood pressure monitoring devices. *Computing in Cardiology (CinC)*, *38*, 593–596.

Chabat, F., Yang, G., & Hansell, D. (2003). Obstructive lung diseases: texture classification for differentiation at CT Radiology., *228*(3), 871– 877.

Chan, K. L. (1992). Fractal Based Texture Analysis. *Singapore ICCS/ISITA*, 102–106.

Chang, C. C., & Lin, C. J. (2016). LIBSVM - A Library for Support Vector Machines. Retrieved from https://www.csie.ntu.edu.tw/~cjlin/libsvm/.

Chaudhuri, B. B., & Sarkar, N. (1995). Texture segmentation using fractal dimension. *IEEE Transactions on Pattern Analysis and Machine Intelligence*, *l7*(1), 72–77. doi:10.1109/34.368149

Chen C.C., Daponte, J.S., & Fox, M.D. (1989), Fractal feature analysis and classification in medical imaging, *IEEE Trans. on Medical Imaging*, 8(2), 133-142.

Chen, H., Sun, X., Chen, H., Wu, Z., & Wang, B. (2004). Some problems in multifractal spectrum computation using a statistical method. *New Journal of Physics*, *84*, 1–17. doi:10.1088/1367-2630/6/1/084

Chhabra, A., & Jensen, R. V. (1989). Physical Review letters. *Direct Determination of the F(alpha) Singularity Spectrum*, *62*(March), 1327– 1330.

Choi, E., & Lee, C. (2003). Feature extraction based on the Bhattacharyya distance. *The Journal of the Pattern Recognition Society*, *36*, 1703–1709. doi:http://10.1016/S0031-3203(03)00035-9

Clarke, K. C. (1986). Computation of the fractal dimension of topographic surfaces using the triangular prism surface area method. *Computers & Geosciences*, *l2*(5), 713–722. doi:10.1016/0098-3004(86)90047-6

Cosatto, V. F., Liew, G., Rochtchina, E., Wainwright, A., Zhang, Y., Hsu, W., … Wang, J. J. (2010). Retinal vascular fractal dimension measurement and its influence from imaging variation: results of two segmentation methods. *Current Eye Research*, *35*(9), 850–856. doi:10.3109/02713683.2010.490628

Dan, Z., Chen, Y., Yang, Z., & Wu, G. (2014). An improved local binary pattern for texture classification. *Optik - International Journal for Light and Electron Optics*, *l25*(20),6320–6324. doi:10.1016/j.ijleo.2014.08.003

Demir, B., Bovolo, F., & Bruzzone, L. (2013). Sequential cascade classification of image time series by exploiting multiple pairwise change detection. *IGARSS*, 3946–3949.

Demšar, J., & Demšar, J. (2006). Statistical Comparisons of Classifiers over Multiple Data Sets. *The Journal of Machine Learning Research*, *7*, 1–30. doi:10.1016/j.jecp.2010.03.005

Demšar, J., Leban, G., & Zupan, B. (2005). Freeviz-an intelligent visualization approach for class-labeled multidimensional data sets. *Proceedings of IDAMAP*, *l*, 13–18.

Dharmagunawardhana, C., & Mahmoodi, S. (2014). Quantitative analysis of pulmonary emphysema using isotropic Gaussian Markov random fields, 44–53. Retrieved from http://eprints.soton.ac.uk/360198/

Ding, Y., Dai, H., & Zhang, H. (2014). Automatic detection of microcalcifications with multifractal spectrum. *Bio-Medical Materials and Engineering*, *24*, 3049–3054. doi:10.3233/BME-141126

Domingos, P. (1997). On the Optimality of the Simple Bayesian Classifier under Zero-One Loss. *Machine Learning*, *29*, 103–130.

Don, S., Chung, D., Revathy, K., Choi, E., Min, D. (2012). A new approach for mammogram image classification using fractal properties, *Cybernetics and Information Technologies,* 12(2), 69-83.

Doyle, S., Feldman, M., Tomaszewski, J., Shih, N., & Madabhushi, A. (2011). Cascaded Multi-class Pairwise Classifier (CASCAMPA) for Normal, Cancerous,and Cancer

Confounder Classes in Prostrate Histology. *IEEE Intnl. Symposium on Biomedical Imaging*, 715–718.

Dubey, S.R., Singh, S.K., & Singh, R.K. (2016). Local bit-plane decoded pattern: A novel feature descriptor for biomedical image retrieval, *IEEE Jrnl. of Biomedical and Health Informatics*, 20(4), 1139-1147.

Dubuisson, M.-P., & Dubes, R. C. (1994). Efficacy of fractal features in segmenting images of natural textures. *Pattern Recognition Letters*, *l5*(April), 419–431. doi:10.1016/0167-8655(94)90091